Published in final edited form as:
Biochemistry. 2009 March 3; 48(8): 1793–1800. doi:10.1021/bi800968w.

Conserved rhodopsin intradiscal structural motifs mediate stabilization; effects of zinc†

Scott Gleim, **Aleksandar Stojanovic**, **Eric Arehart**, **Daniel Byington**, and **John Hwa***
Departments of Pharmacology & Toxicology and Medicine (Section of Cardiology), Dartmouth Medical School, Hanover, NH, 03755.

Abstract

Retinitis pigmentosa (RP), a neurodegenerative disorder, can arise from single point mutations in rhodopsin, leading to a cascade of protein instability, misfolding, aggregation, rod cell death, retinal degeneration, and ultimately blindness. Divalent cations, such as zinc and copper, have allosteric effects on misfolded aggregates of comparable neurodegenerative disorders including Alzheimer disease, prion diseases, and ALS. We report that two structurally conserved low-affinity zinc coordination motifs, located among a cluster of RP mutations in the intradiscal loop region, mediate dose-dependent rhodopsin destabilization. Disruption of native interactions involving histidines 100 and 195, through site-directed mutagenesis or exogenous zinc coordination, results in significant loss of receptor stability. Furthermore, chelation with EDTA stabilizes the structure of both wild type rhodopsin and the most prevalent rhodopsin RP mutation, $P^{23}H$. These interactions suggest that homeostatic regulation of trace metal concentrations in the rod outer segment of the retina may be important both physiologically and for an important cluster of RP mutations. Furthermore, with a growing awareness of allosteric zinc binding domains on a diverse range of GPCRs, such principles may apply to many other receptors and their associated diseases.

Protein misfolding and aggregation is a shared etiology among many neurodegenerative disorders, including Alzheimer disease, Parkinson disease, familial amyotrophic lateral sclerosis, and transmissible spongiform encephalopathies. Over 100 distinct inherited mutations have been identified in rhodopsin, predominantly resulting in misfolding, aggregation, and cell death, followed by clinical manifestation of the retinal neurodegenerative disorder Retinitis Pigmentosa (RP) [1]. Increasing evidence has demonstrated that biologically important and ubiquitous metals, zinc (Zn^{2+}) and copper (Cu^{2+}), directly bind to the β-amyloid (Alzheimer disease) and prion (transmissible spongiform encephalopathies) proteins, linking the gain of non-native, low-affinity metal binding to progression of these disorders. Moreover, Zn^{2+} promotes aggregation of the highly fibrillogenic prion peptide, PrP106-126 [2] and of β-amyloid [3–5]. Such findings have led to promising clinical investigation of metal protein attenuating compounds, based on clioquinol, as potential therapeutics to mitigate β-amyloid neurotoxicity [6–8].

Numerous studies have identified Zn^{2+} as an allosteric modulator of several GPCRs [9–16], including localization of Zn^{2+} coordination sites to extracellular loops of melanocortin [13, 14], chemokine [15], olfactory [16], and tachykinin [12] receptors. These receptors are located within the central nervous system (CNS), where zinc is predominantly stored in synaptic vesicles as a modulator of neuronal excitability [17], and can be found with acute

†Funding Provided by NIH NHLBI RO1 HL074190-01 and The Karl Kirchgessner Foundation Research Grant

Correspondence should be addressed to John Hwa M.D., Ph.D., Department of Pharmacology & Toxicology, 7650 Remsen, Dartmouth Medical School, Hanover, NH, 03755; Phone: 1-603-650-1813; Fax: 1-603-650-1129; Email: John.Hwa@Dartmouth.edu.

concentrations exceeding 300 μM [18,19], suggesting that Zn^{2+} coordination may represent a conserved mechanism regulating GPCRs in the CNS. In a recent study, we identified an essential high-affinity Zn^{2+} coordination site in the transmembrane domain of rhodopsin [20]. Interestingly, we also identified a low-affinity zinc-associated component that significantly destabilized rhodopsin, an effect specific to zinc and copper [21]. Molecular modeling of the rhodopsin crystal structure, in conjunction with data from our previous study [20], indicate His^{100} and His^{195} in the intradiscal domain of rhodopsin as primary candidates for this Zn^{2+}-mediated effect.

The intradiscal domain of rhodopsin, corresponding to the extracellular domain of related GPCRs, is composed of the N-terminus region (residues 1–33), loop II–III (101–105), loop IV–V (173–198), and loop VI–VII (277–285). Mutations in this region prevent rhodopsin from folding properly *in vitro*, a property which precipitates aggregation in the endoplasmic reticulum (ER) [22,23] and subsequent degradation by retinal pigment epithelial cells *in vivo*. The N-terminus tail plays an important role in rhodopsin folding and trafficking [24, 25], while loop IV–V (173–198) contains Cys^{187}, which forms a highly conserved disulfide bond with Cys^{110} [26,27]. This disulfide linkage is essential for proper folding, stability, and function of rhodopsin [26,28–30]. Interestingly, a cluster of RP mutations occurs in this region, many of which promote formation of alternate disulfide bonding [29]. RP mutations Cys^{110}Ala, Cys^{110}Phe, and Cys^{110}Tyr all form an alternate Cys^{185}-Cys^{187} disulfide bond, lacking 11-*cis*-retinal binding [27,29]. Additionally, formation of an ion pair between Arg^{177} and Asp^{190} located at the ends of the second extracellular loop is critical for folding and stability of dark state rhodopsin [31].

In this study, our goal was to identify and characterize the low-affinity metal coordination sites mediating destabilization, and determine potential influence of this phenomenon on normal and pathological RP rhodopsin. We report that two structural networks in the intradiscal domain surrounding His^{100} and His^{195} are susceptible to pathophysiological changes in trace metal concentrations. Trace metal chelation assisted in stabilizing the most common form of RP mutations Pro^{23}His demonstrating such modality as a possible avenue for therapy in select RP mutations.

EXPERIMENTAL PROCEDURES

Site Directed Mutagenesis and Preparation of Rhodopsin Protein Samples

Amino acid substitutions were introduced into the synthetic rhodopsin gene through PCR mutagenesis, as previously described [32]. For single mutants, a synthetic wild-type rhodopsin gene was used as the template [32]. For the His^{100}Phe/His^{195}Phe double mutant, the His^{195}Phe mutant was synthesized using PCR mutagenesis, followed by mutagenesis of His^{100}Phe using His^{195}Phe as the template. COS-1 cells were transfected with pMT4 vectors carrying the opsin genes. Cells were harvested, opsins regenerated with 11-*cis*-retinal, and rhodopsin proteins purified by immunoaffinity chromatography as previously described [32]. Rhodopsin concentration was determined through UV-Vis spectroscopy (500 nm absorbance) [32].

UV-Visible (UV-Vis) Absorption Spectroscopy

UV-Vis absorption spectra were recorded on a Perkin-Elmer λ-40 UV-Vis spectrophotometer at 2°C, 10°C, or 25°C [32]. Rhodopsin thermal stability was determined by monitoring the decay of the 500 nm absorbance at a constant temperature of 50°C, unless otherwise noted. Protein samples were allowed to equilibrate (approximately 2 minutes) to 50°C prior to acquiring absorption spectra. Absorption spectra were obtained at 5-minute intervals until the 500 nm absorbance decreased to background levels. Initial values of the 500 nm absorbance

were normalized between experiments to account for baseline shifts and differences in sample protein concentrations (approximately 1.3 μM).

Computer Modeling

The rhodopsin crystal structures (PDB ID: 1L9H [33] and 1U19 [34]) were visualized with Swiss PDB Viewer (GlaxoSmithKline, Geneva, Switzerland) [35], with some images generated using WebLab Viewer Pro 3.2 (Molecular Simulations, Inc. San Diego, CA). In some models, as described, particular residues were altered from their crystallized structure to propose alternate interactions.

Data Analysis

Values for all experiments are expressed as mean ± SEM. All means and SEM were calculated from at least three distinct experiments using separate protein preparations. Exponential decay rate constants (k) and half-lives were derived through nonlinear regression using GraphPad Prism® software. A 95% confidence interval was used for all curve-fitting procedures using GraphPad Prism. Where applicable, statistical significance of the data was evaluated using an ANOVA and/or unpaired *t* test (*, $p<.05$; **, $p<0.01$; ***, $p<0.001$).

RESULTS

Wild-type rhodopsin becomes less thermostable in the presence of exogenous zinc (Figure 1A). Chelative treatment with 1 mM EDTA stabilized the wild-type rhodopsin receptor (Figure 1A). In a recent study, using inductively coupled plasma mass spectrometry (ICP-MS), we quantified 1.33 ± 0.27 Zn^{2+} ions per molecule of rhodopsin under 10 μM treatment conditions [20]. This suggested the presence of other lower affinity sites, in addition to the single high affinity transmembrane site identified [20]. Moreover, despite the use of approximately 100 mM zinc in the crystallization procedure, the presence of additional sites are supported by rhodopsin's crystal structure [33, 36, 37]. To confirm that other physiologically relevant sites are present, we performed a zinc dose response (thermostability) and calculated the zinc log (EC_{50}) for the alternative site/s to be 1.76 ± 0.08 (log[Zn^{2+}] μM), corresponding to an EC_{50} of 57.1 μM (Figure 1B), confirming both specificity, and the low affinity nature for these additional zinc binding sites. This is consistent with previous findings, and supports the identification of greater than one zinc per rhodopsin molecule detected using ICP–MS [20]. A pH profile for thermostability confirmed a pKA of ~6.7, supporting the possible involvement of His in zinc coordination (Figure 1C). Our goals were then to precisely identify the site/s, determine mechanism for their actions, and determine whether they may be relevant to *Retinitis Pigmentosa* rhodopsin mutations.

Analysis of the Rhodopsin Crystal Structure Indicates His^{100} and His^{195} as Potential Sites of Zn^{2+} Coordination

From the four sites depicting Zn^{2+} coordination in the crystal structure [33], combined with our previous data [20], the sites containing histidine residues His^{100} and His^{195} provide the only suitable candidates for Zn^{2+} coordination. The lack of a histidine, cysteine, or aspartic acid residue at one of the potential Zn^{2+} binding sites, predicted to be formed by Glu^{201} and Gln^{279}, suggests this site to be artifactual (Figure 2A). Based on our pH-profile analysis of receptor stability and zinc-destabilization, histidines are critical to the zinc response. The two remaining sites (Figures 2B and 2C) each contain a histidine residue (His^{100} and His^{195}, respectively). In the rhodopsin crystal structure, one Zn^{2+} ion is located at the dimeric interface between the two rhodopsin monomers, coordinated by Tyr^{96} and His^{100} (from one monomer "a"), Lys^{311} and a backbone amine group from the peptide bond between Gly^{329} and Asp^{330} (from the second monomer "b"; Figure 2B). As tyrosine and lysine are inadequate for zinc

coordination, attention focused on the corresponding histidine (His^{100}) in the intradiscal domain of rhodopsin. Additionally, His^{100} is in proximity of other polar residues, allowing for alternate interactions conceivably masked by the presence of zinc. As such, both His^{100} and His^{195} were suitable candidates for further analysis.

We based our evaluation of the intradiscal hydrogen bonding network on the 1L9H and 1U19 rhodopsin structures. Of the other available rhodopsin crystal structures (PDB: 1F88, 1HZX, 1GZM, 3C9L, and 3C9M), evaluations of 1HZX and 3C9L were included in our initial assessment, and deemed suitably consistent to continue with our current working model. Our focus on the Okada rhodopsin structures, despite the availability of additional structures, was based on the other published structures having removed divalent cations in post-processing, leaving manually inserted water molecules in their place. The substantial resolution of the structures by Okada et al. strengthened and supported our decision.

His^{100} mediates the destabilization conferred by trace metals

Of the 102 sequenced vertebrate type I opsin proteins (GPCRdb [38]), His^{100} is highly conserved, present in 79% of the sequences (Figure 3A), followed by asparagines (19%). Histidine and asparagine, each possess a protonatable nitrogen at the delta position. Interestingly, the remaining 2% of sequences contain nitrogen at the epsilon position, suggesting complete conservation of this functional group among vertebrate type I opsins. We initially performed site-directed mutagenesis of His^{100} to a similarly sized phenylalanine, lacking the polarity to coordinate Zn^{2+}, or to form hydrogen bonds. There was no significant difference in the ability of His^{100}Phe rhodopsin to bind 11-*cis*-retinal at 25°C, as the A_{280}/A_{500} ratio and absorbance maxima of 2.0 similar to wild-type (WT) (Supplement Figure 2). When we treated wild-type rhodopsin with 50 μM $ZnCl_2$ (EC_{50} concentration), rhodopsin decayed at an increased rate of $0.044 \pm 0.002\ min^{-1}$ (WT = $0.026 \pm 0.002\ min^{-1}$, a ratio of 1.69, $p<0.001$; Figure 3C). The *k* rate constant of rhodopsin decay also increased from $0.026 \pm 0.002\ min^{-1}$ for wild-type rhodopsin to $0.057 \pm 0.005\ min^{-1}$ for His^{100}Phe (H100F) (a ratio of 2.19, $p<0.001$). Additionally, comparing the H^{100}-related decay curves with a two-way ANOVA confirms their significance ($p<0.001$). These data indicate that disruption of His^{100}-mediated interactions, through site-directed mutagenesis, results in rhodopsin destabilization similar to Zn^{2+} treatment. Treating His^{100}Phe with 50 μM $ZnCl_2$, led to further destabilization, decaying at an accelerated rate of $0.084 \pm 0.009\ min^{-1}$, compared to the initial rate of $0.057 \pm 0.005\ min^{-1}$ for His^{100}Phe alone (a ratio of 1.47, $p<0.05$). The similar level of destabilization between His^{100}Phe and wild-type treated with zinc supports the notion of His^{100} involvement; however, additional loss of receptor thermostability with post-mutational addition of zinc suggests that either an additional or alternative site is directly involved in the observed zinc-mediated destabilization.

Crystal Structure Analysis Indicates the Presence of a Highly Conserved Hydrogen-Bonding Network Coordinated by His^{100}

Disrupting the receptor structure with zinc or mutagenesis, at position 100, impairs receptor stability, suggesting important native interactions with proximal amino acids. We identified Tyr^{96} (100% conserved in transmembrane domain II) and Tyr^{102} (93% conserved in extracellular loop II) as likely candidates (Figure 3B). A Tyr-His-Tyr triad appears in 79% of the vertebrate opsins and in each opsin containing a His^{100} residue, with tyrosine 96 having 93% conservation and tyrosine 102 completely conserved (Figure 3A). Extending this evaluation beyond simple sequence conservation to the relative position of functional groups supports the hypothesis of regional structural preservation. Threonine has 88% conservation at position 97, with the remaining sequences possessing serine at this site, resulting in 100%

conservation of the gamma-hydroxyl functional group. Interestingly, position 101 maintains 100% conservation of small flexible Gly or Ala residues.

His^{195} additionally mediates trace metal regulated thermostability

Further receptor destabilization with addition of zinc to His^{100}Phe suggests that another site also contributes to the effect. An alternative extracellular histidine (His^{195}) was similarly characterized using site-directed mutagenesis and thermal stability assessment. In contrast to His^{100}, His^{195} is unique to bovine rhodopsin (the source of the crystal structure), with a lysine residue at this position in human rhodopsin. Lysine is 42% conserved at position 195 across type I vertebrate opsins, second only to alanine (44%) (Figure 4A). His^{195}Phe and His^{195}Lys showed no significant difference in the ability to bind 11-*cis*-retinal at 25°C, with an absorbance ratio similar to wild-type (WT). Both His^{195}Phe and His^{195}Lys mutations destabilized rhodopsin less dramatically than mutation of His^{100}. Interestingly, while His^{195}Lys was less stable than WT, this mutation also reduced the destabilizing impact of zinc treatment. The *k* rate constant of rhodopsin decay increased from the wild-type ($0.026 \pm 0.002\ min^{-1}$) to $0.037 \pm 0.005\ min^{-1}$ for His^{195}Lys and $0.069 \pm 0.005\ min^{-1}$ (a ratio of 2.65, $p<0.0001$) for His^{195}Phe (Figure 4C). As before, comparing the collection of decay curves using a two-way ANOVA confirms their significance ($p<0.001$), and suggest that, as with His^{100}, disruption of His^{195} also mediates the destabilizing effects observed with $ZnCl_2$ treatment. To evaluate involvement of His^{195} in metal coordination, we treated these two rhodopsin mutants (His^{195}Phe and His^{195}Lys) with $ZnCl_2$. Both mutants demonstrated elevated destabilization with Zn^{2+} treatment, though this effect was modest for His^{195}Lys. The His^{195}Lys mutant, decayed at a rate of $0.037 \pm 0.005\ min^{-1}$, with an increased rate of $0.042 \pm 0.003\ min^{-1}$ upon addition of 50 μM $ZnCl_2$. The His^{195}Phe mutant decayed at a rate of $0.069 \pm 0.005\ min^{-1}$, compared to an accelerated rate of $0.087 \pm 0.005\ min^{-1}$ (a ratio of 1.26, $p<0.05$) when treated with 50 μM $ZnCl_2$. Not surprisingly, His^{195}Lys remains a great deal more stable than His^{195}Phe, as it retains similar polarity to the native bovine rhodopsin histidine, again highlighting important intradiscal interactions involving the residue at this position. Interestingly, the observed differences between His^{195} and His^{195}Lys suggest that, while Lys^{195} is less stable than His^{195}, it may provide some degree of protection from additional structural instability induced by zinc association.

Opsin Sequence Analysis Supports the Presence of a Conserved Interaction between Residues 195 and 197

Sequence analysis indicates the His^{195}-Glu^{197} pair to be unique to bovine rhodopsin, however a Lys^{195}-Glu^{197} pair is 32% conserved across the vertebrate opsins including human rhodopsin (Figure 4A). Beginning at residue 194, a motif of LKPEV accounts for 31% of all type I vertebrate opsins with RAEGF accounting for 35%. Taken together, a motif of (R^{194}/K^{195})xE is 82% conserved. Phylogenic distribution of these structural motifs, among type I vertebrate opsins, reveals segregation between land (LKPEV dominant) and aquatic (RAEGF dominant) vertebrates. Modeling illustrates that the LKPEV motif maintains a pocket capable of accommodating zinc-coordination, whereas the RAEGF motif may not (Figure 4B). Bovine rhodopsin is unique at this position, containing a PHEET motif. Furthermore, our study suggests that disrupting this interaction, through site-directed mutagenesis or zinc coordination, alters the structure of this region resulting in dramatic protein instability. This instability may very occur through subsequent disruption of the proposed ion pair between Arg^{177} and Asp^{190} (Figure 4A and 4B) located at the ends of the second extracellular loop which is critical for folding and stability of dark state rhodopsin [31].

The $His^{100}Phe/His^{195}Phe$ Double-Mutant is unaffected by further zinc treatment

To evaluate whether these histidines are sufficient to mediate the observed Zn^{2+}-induced instability, we constructed the $His^{100}Phe/His^{195}Phe$ double-mutant rhodopsin protein. The $His^{100}Phe/His^{195}Phe$ mutant displayed reduced 11-*cis*-retinal binding at 25°C. Thermal stability of the $His^{100}Phe/His^{195}Phe$ double-mutant (Figure 5), with an accelerated decay rate of $0.277 \pm 0.027\ min^{-1}$, demonstrated dramatic impact on protein stability relative to wild-type rhodopsin ($0.026 \pm 0.002\ min^{-1}$) (a ratio of 10.65, $p<0.0001$),. The resulting instability appears to be synergistic, as each individual mutation accounts for less than half the observed decay rate ($His^{100}Phe$ at $0.057 \pm 0.005\ min^{-1}$ and $His^{195}Phe$ at $0.069 \pm 0.005\ min^{-1}$). There was no statistically significant difference between the $His^{100}Phe/His^{195}Phe$ double-mutant treated with 50 μM $ZnCl_2$ that decayed at a rate of $0.225 \pm 0.023\ min^{-1}$ and the untreated double-mutant, which decayed at a rate of $0.277 \pm 0.027\ min^{-1}$ ($p>0.05$; ns; Figure 5A), supporting the identification of the critical zinc coordination sites. Further studies were performed at 37°C to assess whether there were any significant differences at a lower temperature where rhodopsin would be more stable (Figure 5B). As expected the double mutant receptor demonstrated increased stability at 37°C ($0.144 \pm 0.017\ min^{-1}$) compared to 50°C. Consistent with the higher temperature experiments, the addition of 50 μM Zn^{2+} ($0.165 \pm 0.015\ min^{-1}$) or 1 mM EDTA ($0.155 \pm 0.016\ min^{-1}$) made no further impact on the double mutant. These results support both His^{100} and His^{195} as critical rhodopsin stabilizing sites which are exquisitely sensitive to destabilization by zinc coordination.

Chelation of trace Zn^{2+} can stabilize *Retinitis Pigmentosa* mutation $Pro^{23}His$

As exogenous zinc demonstrated a physiological role in modulating rhodopsin structural stability, we hypothesized that it may additionally play a role for structurally impaired RP mutants. Wild-type rhodopsin treated with EDTA showed significant thermal stabilization (Figure 1A). The $Pro^{23}His$ rhodopsin mutation (most common RP mutations in North America) results in a structure significantly less stable than WT rhodopsin, with a decay rate of $0.450 \pm 0.032\ min^{-1}$. Pre-treatment of $Pro^{23}His$ rhodopsin with 1 mM EDTA significantly increases receptor thermostability ($0.173 \pm 0.021\ min^{-1}$) at high temperature (a ratio of 2.60, $p<0.05$; Figure 6A). Although this corresponds to greater than a two-fold increase in receptor half-life, the rapidity of receptor unfolding at this high temperature results in a low resolution of decay rates for highly unstable forms of rhodopsin like $Pro^{23}His$. To increase resolution of this observation, a lower temperature (37°C) demonstrates enhanced stability, with a decay rate of 0.122 ± 0.012 for $Pro^{23}His$, increasing to 0.027 ± 0.007 with 1 mM EDTA treatment (a ratio of 4.52, $p<0.05$; Figure 6B). This difference corresponds to more than a four-fold increase in receptor half-life. We hypothesize that as with wild type, EDTA chelation stabilizes the $Pro^{23}His$ through prevention of zinc coordination at the native His^{100}, $His^{195}Phe$ sites. We cannot exclude the formation of a third zinc binding site involving $Pro^{23}His$, though we surmise that zinc can similarly influence intradiscal RP mutations and may therefore play a role in disease progression and therapy.

DISCUSSION

Allosteric effects of trace metals on G-protein coupled receptors have demonstrated implications in both health and disease [9–16,39,40]. Trace metals such as zinc can accumulate to high concentrations within organs and subcellular compartments [41], influencing many neurodegenerative diseases [2–4,41,42]. The rhodopsin crystal structure provides a unique opportunity to elucidate precise mechanisms of allosteric action. This ultimately can serve to establish important principles for other GPCRs.

Zinc binding has dual and opposing roles

Rhodopsin displays differential responses to zinc: Transmembrane coordination helps stabilize the receptor [20] and intradiscal coordination appears to destabilize purified rhodopsin (current study). Dual zinc association (His^{100} and His^{195}) within the intradiscal region mediates disruption of receptor thermostability through low-affinity histidine coordination. Significant conservation surrounds the His^{100} zinc-coordinating region, in contrast to His^{195}, which is unique to bovine rhodopsin. Simultaneous replacement of these groups with phenylalanine results in severe structural impairment and eliminates further metal-induced destabilization. Interestingly, human Lys^{195} appears to assist structural integrity in this region, reducing wild type rhodopsin susceptibility to metal interference in comparison to bovine rhodopsin.

With sensitivity to zinc in the physiological range (as observed from our dose response) and evidence of a gradient free zinc distribution within the rod cell itself (high ER concentrations, low in outer segment, and very high in the RPE) [43], we speculate that the observed destabilization may serve both physiological and pathological roles. The high zinc concentrations around the ER may be involved in rhodopsin folding (or dimerization as proposed by Park et al [44]), particularly with the assistance of chaperonins. The absence of available free zinc across the outer segment (as with our EDTA experiments) imposes maximal stability and thus optimal rhodopsin function. Finally, high zinc concentrations observed in the RPE may assist in the destabilizing, unfolding, and proteolytic degradation of rhodopsin. In the absence of chaperonins or proteolytic cleavage, instability arising from zinc coordination may promote oligomerization and/or aggregation. Formation of stable oligomers is supported by previous scanning force microscopy (SFM) data suggesting that zinc-coordination promotes self-association of the photoreceptor [44].

Implications for Retinitis Pigmentosa

Our findings with the most prevalent rhodopsin RP mutation, $Pro^{23}His$, support a potential pathological involvement of zinc-coordination in rhodopsin. In the context of *retinitis pigmentosa*, the impairment of receptor integrity observed with trace metal coordination would accelerate the progression of disease. Specific RP mutations, particularly those among the intradiscal region, may amplify the impact of metal-induced destabilization. The instability of $Pro^{23}His$ may be related to potential aberrant Zn-binding sites, or influence the known sites, in addition to effects on the native disulfide bond. Unfortunately, misfolding and aggregation currently prevents accurate assessments of these possibilities. Although chelative zinc removal does not completely restore the $P^{23}H$ photoreceptor to wild-type stability levels, half-life increases of three-fold to five-fold may be suitable to slow the progression of retinal degeneration. The impact of structural impairment in RP progression, coupled with metal-induced misfolding, permits speculation regarding the possibility for chelative agents to inhibit disease progression. Metal protein attenuating compounds, such as PBT2 [45], are being developed and evaluated for utility in chelating metals from protein aggregates. Though currently focused on Alzheimers plaques, if analogs can distribute, or be delivered, to photoreceptors they may be useful in a subset of RP mutants. The influence of metal-coordination on rhodopsin structural integrity extends insight into native receptor structure, enhancing general understanding of GPCRs, and may point toward potential therapeutics.

Supplementary Material

Refer to Web version on PubMed Central for supplementary material.

Glossary

Abbreviations

A_{500}
absorbance at 500nm

ANOVA
analysis of variance

ED_{50}
half maximal effective dose

EDTA
ethylenediaminetetraacetic acid

GPCR
G-protein coupled receptor

His
histidine

ICP-MS
inductively coupled plasma mass spectrometry

Lys
lysine

Phe
phenylalanine

pKa
acid dissociation constant

Pro
proline

RP
Retinitis Pigmentosa

SDS
sodium dodecyl sulfate

SEM
standard error of the mean

SFM
scanning force microscopy

Tyr
tyrosine

UV-Vis
ultraviolet-visible

WT
wild-type

Zn
zinc

References

1. Stojanovic A, Hwa J. Rhodopsin and retinitis pigmentosa: shedding light on structure and function. Receptors Channels 2002;8(1):33–50. [PubMed: 12402507]
2. Jobling MF, et al. Copper and zinc binding modulates the aggregation and neurotoxic properties of the prion peptide PrP106-126. Biochemistry 2001;40(27):8073–8084. [PubMed: 11434776]
3. Atwood CS, et al. Dramatic aggregation of Alzheimer abeta by Cu(II) is induced by conditions representing physiological acidosis. J Biol Chem 1998;273(21):12817–12826. [PubMed: 9582309]
4. Huang X, et al. Zinc-induced Alzheimer's Abeta1-40 aggregation is mediated by conformational factors. J Biol Chem 1997;272(42):26464–26470. [PubMed: 9334223]
5. Lynch T, Cherny RA, Bush AI. Oxidative processes in Alzheimer's disease: the role of abeta-metal interactions. Exp Gerontol 2000;35(4):445–451. [PubMed: 10959032]
6. Doraiswamy PM, Xiong GL. Pharmacological strategies for the prevention of Alzheimer's disease. Expert Opinion on Pharmacotherapy 2006;7(1):1–10. [PubMed: 16370917]
7. Ritchie CW, Bush AI, Masters CL. Metal-protein attenuating compounds and Alzheimer's disease. Expert Opinion on Investigational Drugs 2004;13(12):1585–1592. [PubMed: 15566316]
8. Finefrock AE, Bush AI, Doraiswamy PM. Current status of metals as therapeutic targets in Alzheimer's disease. J Am Geriatr Soc 2003;51(8):1143–1148. [PubMed: 12890080]
9. Schetz JA, Sibley DR. Zinc allosterically modulates antagonist binding to cloned D1 and D2 dopamine receptors. J Neurochem 1997;68(5):1990–1997. [PubMed: 9109525]
10. Swaminath G, Lee TW, Kobilka B. Identification of an allosteric binding site for Zn2+ on the beta2 adrenergic receptor. J Biol Chem 2003;278(1):352–356. [PubMed: 12409304]
11. Swaminath G, et al. Allosteric modulation of beta2-adrenergic receptor by Zn(2+). Mol Pharmacol 2002;61(1):65–72. [PubMed: 11752207]
12. Rosenkilde MM, et al. Natural agonist enhancing bis-His zinc-site in transmembrane segment V of the tachykinin NK3 receptor. FEBS Lett 1998;439(1–2):35–40. [PubMed: 9849872]
13. Holst B, Elling CE, Schwartz TW. Metal ion-mediated agonism and agonist enhancement in melanocortin MC1 and MC4 receptors. J Biol Chem 2002;277(49):47662–47670. [PubMed: 12244039]
14. Holst B, Schwartz TW. Molecular mechanism of agonism and inverse agonism in the melanocortin receptors: Zn(2+) as a structural and functional probe. Ann N Y Acad Sci 2003;994:1–11. [PubMed: 12851292]
15. Gerlach LO, et al. Metal ion enhanced binding of AMD3100 to Asp262 in the CXCR4 receptor. Biochemistry 2003;42(3):710–717. [PubMed: 12534283]
16. Wang J, Luthey-Schulten ZA, Suslick KS. Is the olfactory receptor a metalloprotein? Proc Natl Acad Sci U S A 2003;100(6):3035–3039. [PubMed: 12610211]
17. Frederickson CJ, et al. Importance of Zinc in the Central Nervous System: The Zinc-Containing Neuron. J. Nutr 2000;130(5):1471S–1483S. [PubMed: 10801962]
18. Howell GA, Welch MG, Frederickson CJ. Stimulation-induced uptake and release of zinc in hippocampal slices. Nature 1984;308(5961):736–738. [PubMed: 6717567]
19. Assaf SY, Chung S-H. Release of endogenous Zn2+ from brain tissue during activity. Nature 1984;308(5961):734–736. [PubMed: 6717566]
20. Stojanovic A, Stitham J, Hwa J. Critical role of transmembrane segment zinc binding in the structure and function of rhodopsin. J Biol Chem 2004;279(34):35932–35941. [PubMed: 15194703]
21. del Valle LJ, et al. Zinc-induced Decrease of the Thermal Stability and Regeneration of Rhodopsin. J. Biol. Chem 2003;278(7):4719–4724. [PubMed: 12482872]
22. Sung CH, et al. Rhodopsin mutations in autosomal dominant retinitis pigmentosa. Proc Natl Acad Sci U S A 1991;88(15):6481–6485. [PubMed: 1862076]
23. Olsson JE, et al. Transgenic mice with a rhodopsin mutation (Pro23His): a mouse model of autosomal dominant retinitis pigmentosa. Neuron 1992;9(5):815–830. [PubMed: 1418997]
24. Borjigin J, Nathans J. Insertional mutagenesis as a probe of rhodopsin's topography, stability, and activity. J Biol Chem 1994;269(20):14715–14722. [PubMed: 7514180]

25. Doi T, Molday RS, Khorana HG. Role of the intradiscal domain in rhodopsin assembly and function. Proc Natl Acad Sci U S A 1990;87(13):4991–4995. [PubMed: 2367520]
26. Karnik SS, Khorana HG. Assembly of functional rhodopsin requires a disulfide bond between cysteine residues 110 and 187. J Biol Chem 1990;265(29):17520–17524. [PubMed: 2145276]
27. Hwa J, Klein-Seetharaman J, Khorana HG. Structure and function in rhodopsin: Mass spectrometric identification of the abnormal intradiscal disulfide bond in misfolded retinitis pigmentosa mutants. Proc Natl Acad Sci U S A 2001;98(9):4872–4876. [PubMed: 11320236]
28. Karnik SS, et al. Cysteine residues 110 and 187 are essential for the formation of correct structure in bovine rhodopsin. Proc Natl Acad Sci U S A 1988;85(22):8459–8463. [PubMed: 3186735]
29. Hwa J, et al. Structure and function in rhodopsin: further elucidation of the role of the intradiscal cysteines, Cys-110, -185, and -187, in rhodopsin folding and function. Proc Natl Acad Sci U S A 1999;96(5):1932–1935. [PubMed: 10051572]
30. Davidson FF, Loewen PC, Khorana HG. Structure and function in rhodopsin: replacement by alanine of cysteine residues 110 and 187, components of a conserved disulfide bond in rhodopsin, affects the light-activated metarhodopsin II state. Proc Natl Acad Sci U S A 1994;91(9):4029–4033. [PubMed: 8171030]
31. Janz JM, Fay JF, Farrens DL. Stability of Dark State Rhodopsin Is Mediated by a Conserved Ion Pair in Intradiscal Loop E-2. J. Biol. Chem 2003;278(19):16982–16991. [PubMed: 12547830]
32. Stojanovic A, et al. Retinitis pigmentosa rhodopsin mutations L125R and A164V perturb critical interhelical interactions: new insights through compensatory mutations and crystal structure analysis. J Biol Chem 2003;278(40):39020–39028. [PubMed: 12871954]
33. Okada T, et al. Functional role of internal water molecules in rhodopsin revealed by X-ray crystallography. Proc Natl Acad Sci U S A 2002;99(9):5982–5987. [PubMed: 11972040]
34. Okada T, et al. The retinal conformation and its environment in rhodopsin in light of a new 2.2 A crystal structure. J Mol Biol 2004;342:571–583. [PubMed: 15327956]
35. Guex N, Peitsch MC. SWISS-MODEL and the Swiss-PdbViewer: an environment for comparative protein modeling. Electrophoresis 1997;18(15):2714–2723. [PubMed: 9504803]
36. Palczewski K, et al. Crystal structure of rhodopsin: A G protein-coupled receptor. Science 2000;289 (5480):739–745. [PubMed: 10926528]
37. Teller DC, et al. Advances in determination of a high-resolution three-dimensional structure of rhodopsin, a model of g-protein-coupled receptors (gpcrs)(,). Biochemistry 2001;40(26):7761–7772. [PubMed: 11425302]
38. Horn F, et al. GPCRDB information system for G protein-coupled receptors. Nucl. Acids Res 2003;31 (1):294–297. [PubMed: 12520006]
39. Liu Y, et al. Identification of a Zn2+-binding site on the dopamine D2 receptor. Biochemical and Biophysical Research Communications 2006;339(3):873–879. [PubMed: 16332354]
40. Schetz JA, Chu A, Sibley DR. Zinc Modulates Antagonist Interactions with D2-Like Dopamine Receptors through Distinct Molecular Mechanisms. J Pharmacol Exp Ther 1999;289(2):956–964. [PubMed: 10215675]
41. Frederickson CJ, Koh J-Y, Bush AI. The neurobiology of zinc in health and disease 2005;6(6):449–462.
42. Cherny RA, et al. Treatment with a copper-zinc chelator markedly and rapidly inhibits b-amyloid accumulation in Alzheimer's disease transgenic mice. Neuron 2001;30:665–676. [PubMed: 11430801]
43. Akagi T, et al. Differential Subcellular Localization of Zinc in the Rat Retina. J. Histochem. Cytochem 2001;49(1):87–96. [PubMed: 11118481]
44. Park PS-H. Stabilizing Effect of Zn2+ in Native Bovine Rhodopsin. J. Biol. Chem 2007;282(15): 11377–11385. [PubMed: 17303564]
45. Adlard PA, et al. Rapid Restoration of Cognition in Alzheimer's Transgenic Mice with 8-Hydroxy Quinoline Analogs Is Associated with Decreased Interstitial A[beta]. Neuron 2008;59(1):43–55. [PubMed: 18614028]

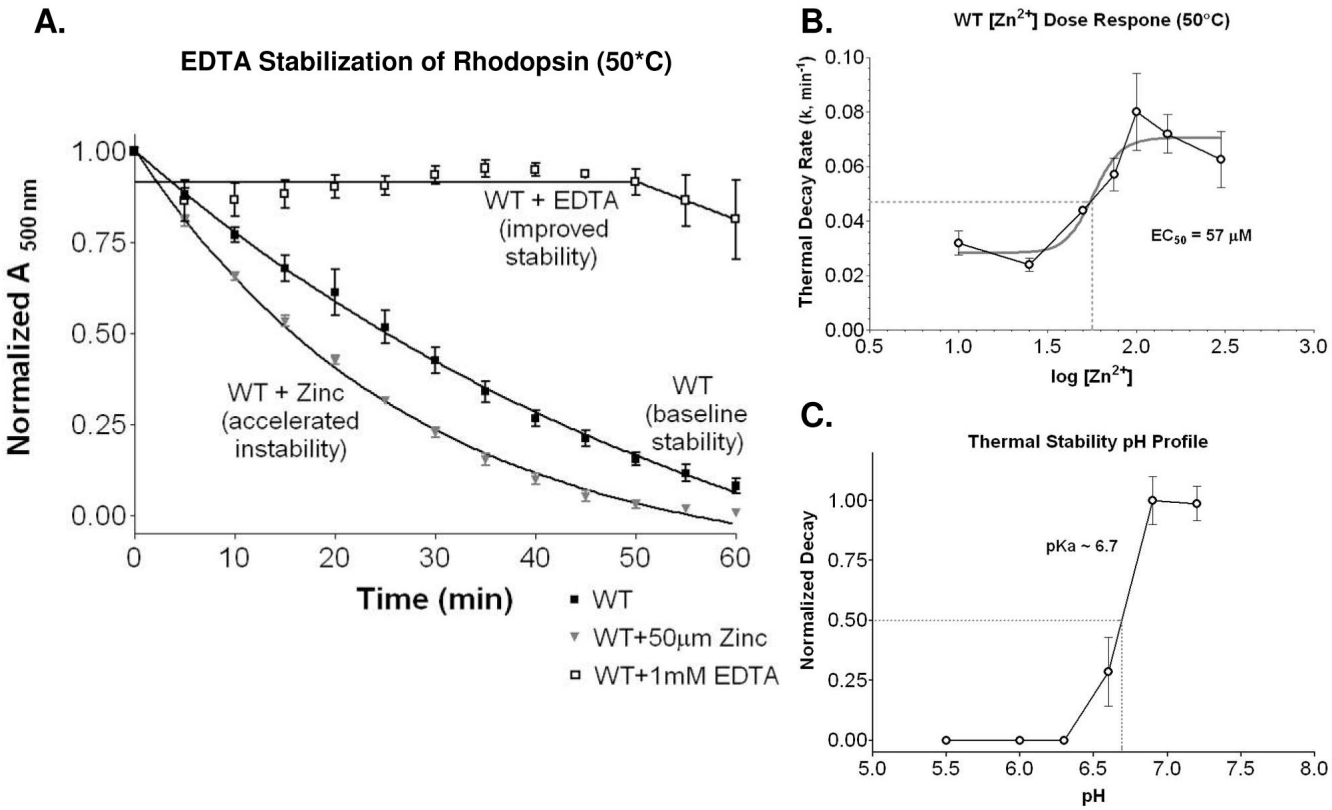

Figure 1.

A. Thermal decay (at 50°C) time course for wild type (WT), wild type plus 50 µM $ZnCl_2$, and wild type treated with 1 mM EDTA. **B**. Dose response relationship of zinc concentrations (log [Zn^{2+}] µM) to receptor thermal decay rate (k). Non-linear regression determined a log(EC_{50}) of 1.76 ± 0.08, corresponding to an EC_{50} of 57.1 µM $ZnCl_2$. **C**. Thermal decay of wild type rhodopsin adopts a pH profile with an apparent pKa of 6.7, consistent with histidine involvement.

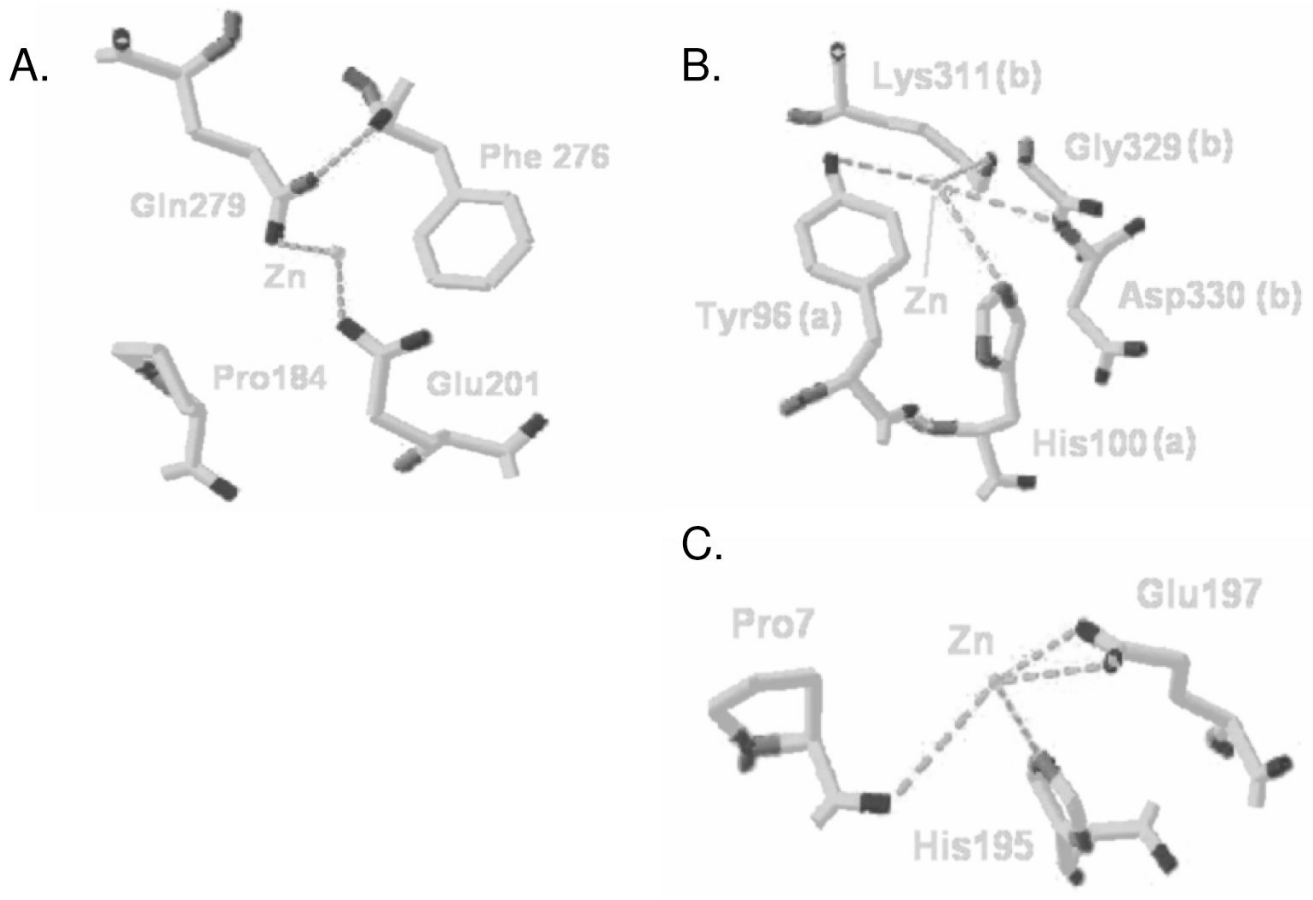

Figure 2.

Three positions (non-transmembrane) illustrating potential zinc-coordination in the rhodopsin crystal structure. **A**. The lack of residues commonly implicated in zinc-coordination at the Gln^{279} site suggests this position to be artifactual. **B**. The interfacial zinc-coordination site centered at His^{100} bridges two inverted monomers (polypeptide chain 'a' and 'b') in the crystal structure. **C**. Zinc coordinated by His^{195} connects the intradiscal loop to the N-terminal chain through Pro^{7}.

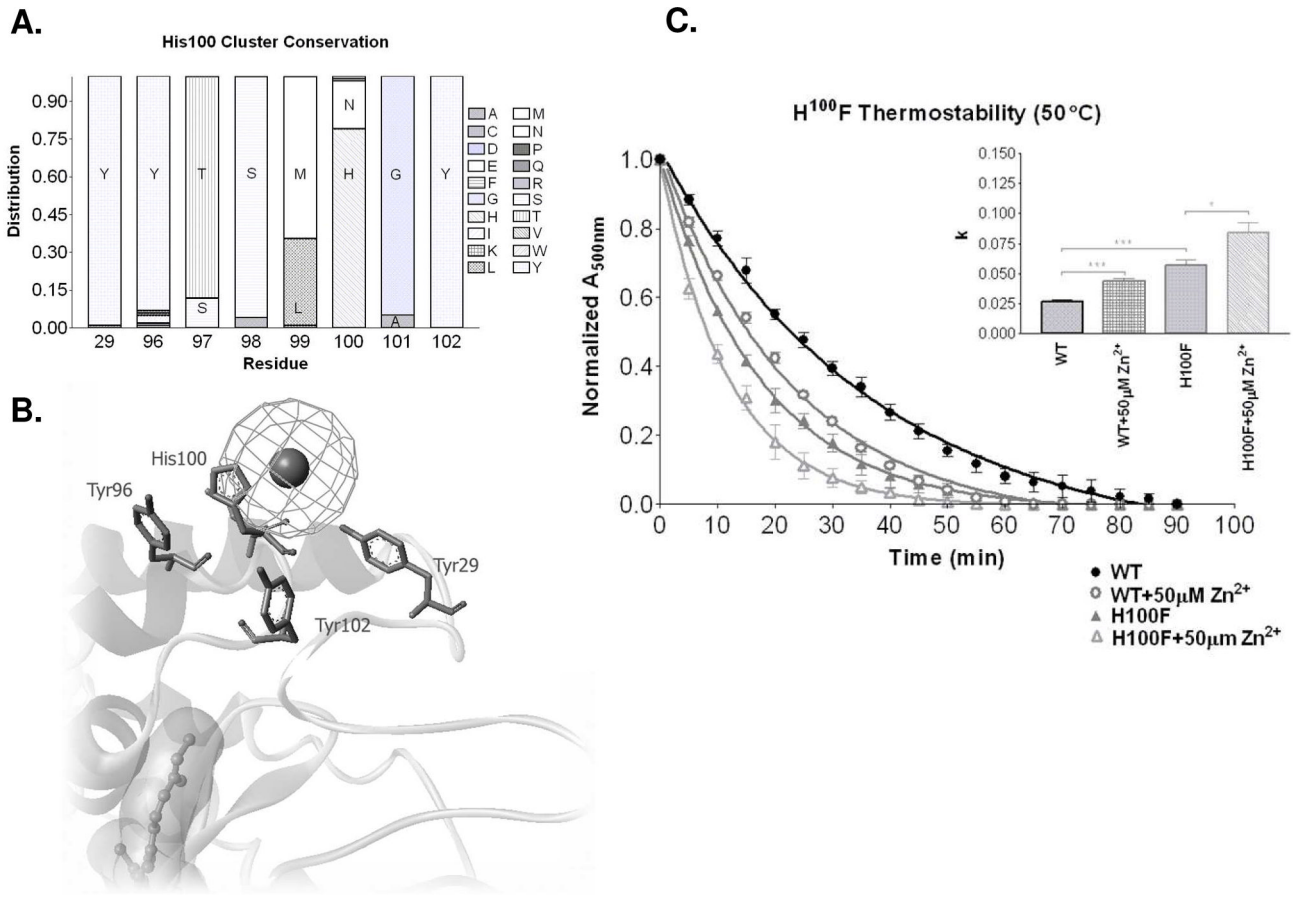

Figure 3.

A. Histogram showing conservation of amino acids at specified residue positions comparing 102 sequenced vertebrate type I opsin proteins (GPCRdb [38]). **B**. The conserved tyrosine residues surround the His^{100} residue in close enough proximity for potential interactions in the presence of zinc (sphere). **C**. The thermal decay rate of wild-type rhodopsin in the presence and absence of 50 μM Zn^{2+}. Thermal decay of $H^{100}F$ is also shown in the presence and absence of 50 μM Zn^{2+}. A bar graph showing the rate constants (k) for each of the constructs and treatments. (* $p<0.05$, *** $p<0.001$). Two-way ANOVA analysis confirmed multi-point significance at $p<0.0001$.

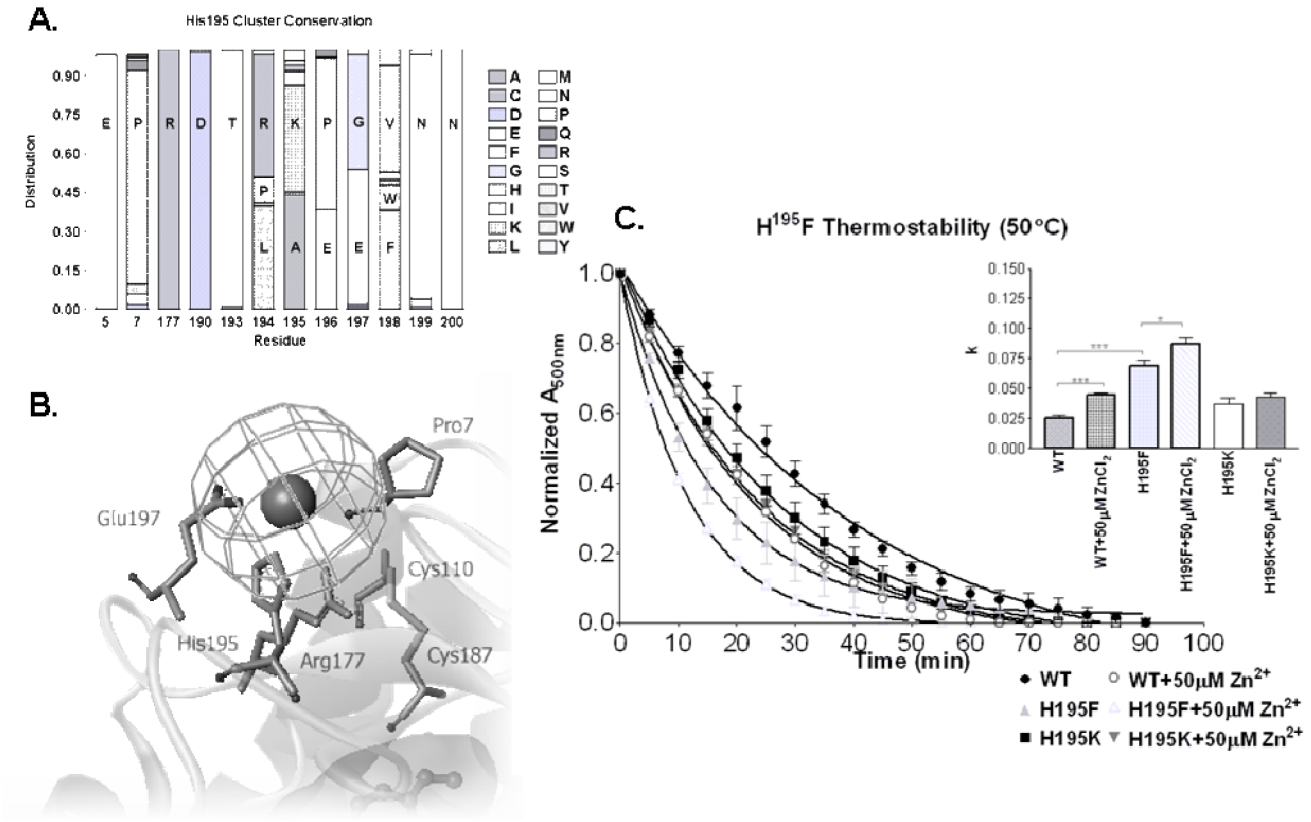

Figure 4.

A. Histogram showing conservation of amino acids at specified residue positions comparing 102 sequenced vertebrate type I opsin proteins (GPCRdb [38]). Sequence divergence follows a motif of [R^{194}/K^{195}]xE, manifest predominantly as LKPEV and RAEGF for land and aquatic vertebrates, respectively. **B**. Charged residues, corresponding to the [R^{194}/K^{195}]xE motif, cluster around His^{195} and the associated zinc in the crystal structure. **C**. The thermal decay rate of wild-type rhodopsin in the presence and absence of 50 μM Zn^{2+}. Thermal decay of $H^{195}F$ and $H^{195}K$ are also shown in the presence and absence of 50 μM Zn^{2+}. The bar graph shows rate constants (k) for each construct and treatment. (* $p<0.05$, *** $p<0.001$). Two-way ANOVA analysis confirmed multi-point significance at $p<0.0001$.

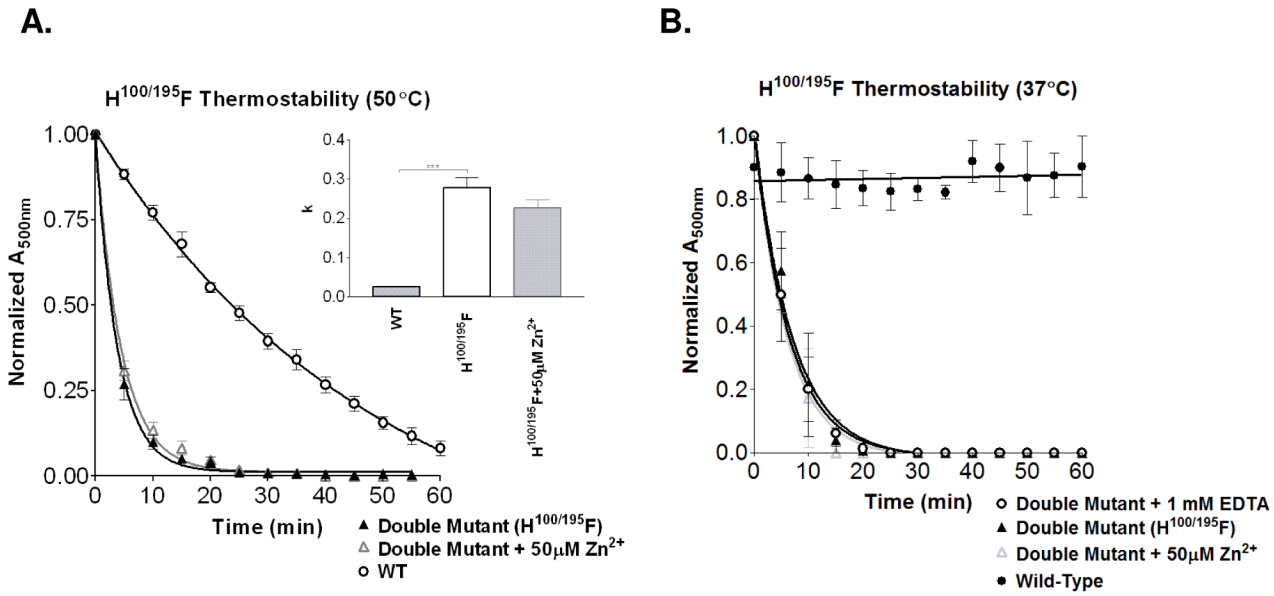

Figure 5.

A. Simultaneous removal of both His^{100} and His^{195} results in a dramatically unstable photoreceptor (0.277 ± 0.027 min^{-1}). Additional treatment of the double mutant with 50 μM zinc has no further impact on thermal stability (0.225 ± 0.023 min^{-1}). Shown in the bar graphs are the respective rate constants (k). (*** $p<0.001$). **B**. The double mutant receptor (0.144 ± 0.017 min^{-1}) evaluated at a lower temperature (37°C) remained consistent with the higher temperature, showing no significant differences in thermal stability with the addition of either 50 μM Zn^{2+} (0.165 ± 0.015 min^{-1}) or 1 mM EDTA (0.155 ± 0.016 min^{-1}).

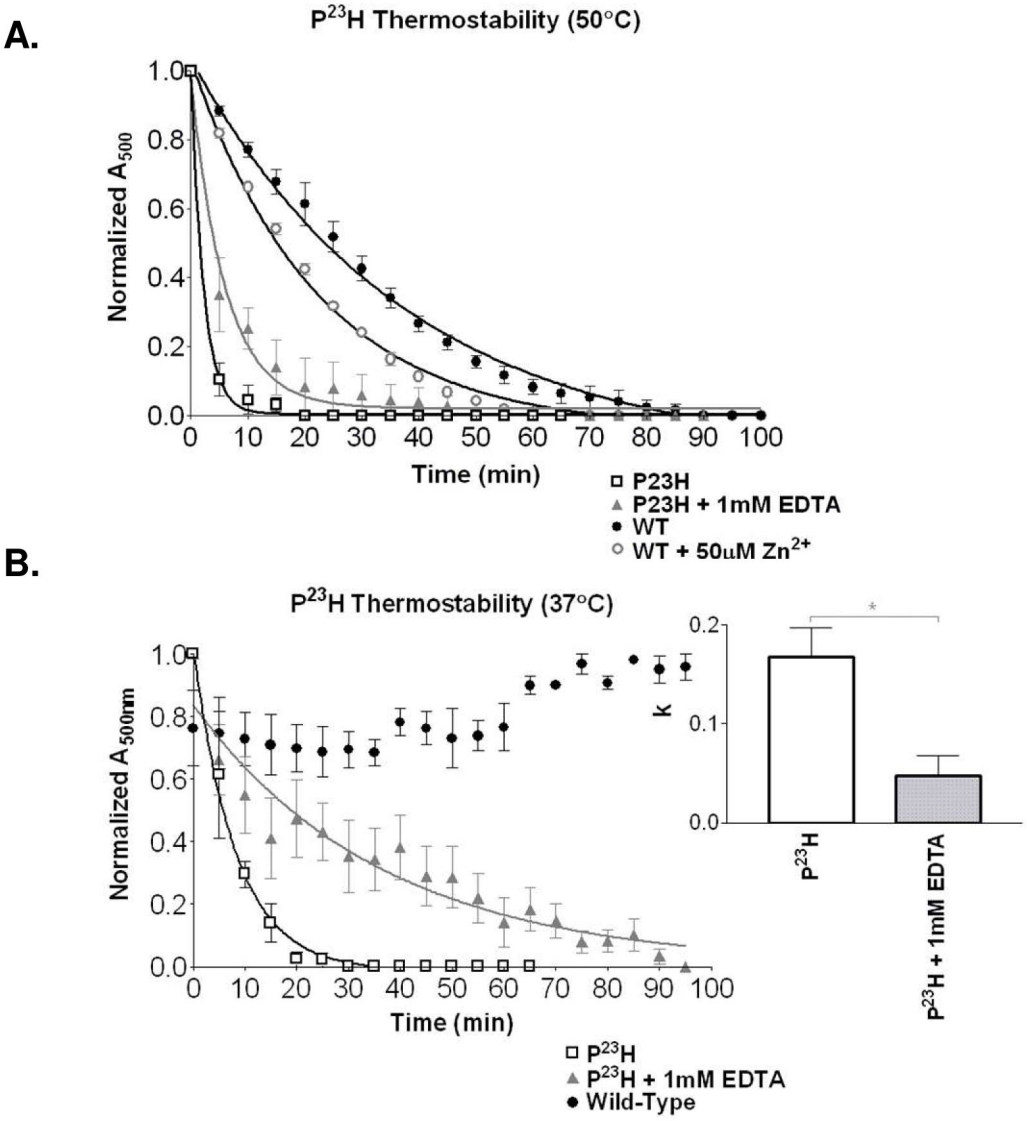

Figure 6.

A. Thermal decay (50°C) for the most prevalent rhodopsin RP mutant, Pro^{23}His in the absence and presence of EDTA. Results are compared to wild type protein in the presence and absence of Zn^{2+}. Wild type plus EDTA is shown in Figure 1B. **B**. Evaluating the unstable mutants at a lower temperature (37°C) improves resolution between the decay curves for Pro^{23}His and the same mutant treated with EDTA. The bar graph illustrates improvement in decay rate (k) with EDTA (* $p<0.05$). Two-way ANOVA analysis confirmed multi-point significance at $p<0.0001$.